www.sciencemag.org/content/351/6269/aad5694/suppl/DC1

Supplementary Materials for

Gating of hippocampal activity, plasticity, and memory by entorhinal cortex long-range inhibition

Jayeeta Basu,* Jeffrey D. Zaremba, Stephanie K. Cheung, Frederick L. Hitti, Boris V. Zemelman, Attila Losonczy, Steven A. Siegelbaum*

*Corresponding author. E-mail:: jayeeta.basu@nyumc.org (J.B.); sas8@columbia.edu (S.A.S.)

Published 8 January 2016, *Science* **351**, aaa5694 (2016)
DOI: 10.1126/science.aad5694

This PDF file includes

Other Supplementary Material for this manuscript includes the following:
(available at www.sciencemag.org/content/351/6269/aad5694/suppl/DC1)

Movie S1

Fig. S1. LEC and MEC GABAergic projections in hippocampus. (**A**) 10X confocal image of a coronal section of right and left hemisphere hippocampi showing ipsilateral expression of tdTomato (magenta) and GFP (green) labeled GABAergic projection axons, following unilateral viral injections in LEC and MEC, respectively. (**B**) 20X confocal projection image showing detailed expression pattern of LEC and MEC LRIPs in hippocampus from injected hemisphere. Note the greater expression of $tdTomato^{+}$ LEC LRIPs in SLM of CA1 compared with GFP^{+} MEC LRIPs, which tend to innervate the outer layer of DG.

Fig. S2. LEC and MEC GABAergic projection pattern in CA1. (**A**) 20X confocal projection image showing LRIPs from LEC (labeled with tdTomato, in magenta) and MEC (labeled with GFP, green) in the hippocampus from the injected hemisphere of a GAD2-Cre mouse injected with AAV^{Cre} expressing tdTomato in LEC and GFP in MEC. (**B**) Schematic of hippocampus with the demarcation of the subfields (subiculum, sub; CA1; CA2; CA3, dentate gyrus-DG), layers (stratum oriens, SO; stratum pyramidale, SP; stratum radiatum, SR and stratum lacunosum moleculare, SLM), and the division along the transverse axis into proximal (CA2 side of CA1), medial (mid CA1) and distal (subicular side of CA1) regions. Bar plots (Mean $\pm$ SEM) quantifying the fluorescence (mean intensity, AU) and spread (% area) of LRIP axons in CA1 originating from LEC [(**C** to **E**) magenta] and MEC [(**F** to **H**) green] in the proximal, medial and distal subdivisions of SLM in CA1. LRIP input from LEC to all regions of CA1 is significantly greater than LRIP input from MEC (using two-tailed *t* tests), based on higher fluorescence intensity (Proximal CA1: LEC = 5991 $\pm$ 489.3 AU versus MEC = 3686 $\pm$ 412.2 AU; $P = 0.0005$; Mid CA1: LEC = 4258 $\pm$ 375.7 AU versus MEC = 1436 $\pm$ 141.6 AU; $P < 0.0001$; Distal CA1: LEC = 3829 $\pm$ 340.4 versus MEC = 1546 $\pm$ 158.8 AU, $P < 0.0001$). LEC LRIPs also covered a larger area of SLM in CA1 compared with MEC LRIPs (LEC = 82.05 $\pm$ 3.64 % of SLM versus MEC = 37.79 $\pm$ 2.35% of SLM; $P < 0.0001$). LEC LRIPs showed a small but significant preference to innervate SLM in proximal versus distal CA1 (Area:

Distal = 79.15 ± 3.98% versus Proximal = 86.68 ± 3.04%; paired *t* test $P < 0.007$). In contrast, MEC LRIPs targeted SLM of proximal CA1 to a greater extent than distal CA1 (proximal = 50.31 ± 2.92% versus distal = 32.04 ± 2.09%; paired *t* test $P < 0.0001$).

Fig. S3. LEC and MEC LRIP connectivity in SLM of CA1. (**A**) Location of the cell bodies of the intracellularly recorded INs at the border of SR/SLM that responded to photostimulation of $ChR2^+$ LRIPs from LEC (magenta circles) and MEC (green rectangles). (**B**) Percentage (%) of intracellularly recorded INs with cell bodies located in the border of SR/SLM of CA1 in which local photostimulation of $ChR2^+$ LRIPs from LEC (53.1% of neurons) versus MEC (32.4% of neurons) produced a light-evoked IPSC. The threshold for a response was set at an IPSC peak amplitude of ≥ 10 pA and a response probability of ≥ 50% per photostimulation episode at 100% laser power. (**C**) Light-evoked IPSC amplitude (pA, mean ± SEM) recorded from CA1 SR/SLM border INs in response to photostimulation of $ChR2^+$ LRIP axons from either MEC or LEC under control conditions (drug-free ACSF, blue; MEC response = 37.74 ± 2.02 pA; LEC response = 139.00 ± 24.5 pA) or in the presence of 10 µM NBQX (green; MEC response = 35.5 ± 1.91 pA; $P = 0.343$ for control versus NBQX, paired *t* test, $n = 10$; LEC response = 138.22 ± 26.7 pA, $P = 0.286$ for control versus NBQX, paired *t* test, $n = 15$) and GABAR blockers (SR 2 µM, CGP 1 µM, red stripes; MEC response = 2.09 ± 1.78 pA, $P < 0.0001$, control versus SR, CGP; LEC response = 1.5 ± 1.69 pA, $P < 0.0001$, control versus. SR, CGP). Note that there is no significant difference between the control and NBQX groups whereas the IPSCs are eliminated upon GABAR blockade, confirming that the LRIPs provide direct GABAergic inputs from MEC and LEC. (**D**) Example trace (left) and mean (± SEM) of light-evoked peak depolarizing PSP amplitude (mV) recorded from CA1 SR/SLM border INs under current clamp conditions at -68 mV in response to photostimulation of $ChR2^+$ LRIP axons from LEC.

Fig. S4. Localization of PSEM and miniRuby to CA1 infusion site in Gad2Cre behavior cohorts. (**A**) Diagram of the experimental design. Gad2-Cre mice were injected with AAV^{Cre} to express GFP or PSAM in LEC. An 0.5 μl volume of PSEM 308 (15 μM) and miniRuby (5% in water) in ACSF was infused into the CA1 region of the hippocampus through a cannula. (**B**) Example confocal image at 5X magnification of a coronal section derived from a Gad2-cre mouse used for behavioral testing that had been injected in LEC with an AAV^{Cre} expressing PSAM-2A-GFP. After infusion of PSEM and miniRuby solution, the mouse was killed, approximately 10 min after the end of the infusion period. Image shows mini Ruby (red), 4′,6′-diamidino-2-phenylindole (DAPI) (blue), and the expression of GFP in LEC (green). (**C**) Higher magnification image showing miniRuby in CA1 restricted to a 1000 μm perimeter spanning the alveus, SO, SP, SR and SLM. (**D**) Image showing absence of detectable miniRuby in LEC, which is positive for GFP (green) and DAPI (blue). The spread of miniRuby provides a likely upper limit of diffusion during the time course of the experiment as PSEM is rapidly metabolized, with an effect limited to 20 min after application [personal communication S. Sternson; (*28*)]. In contrast, miniRuby was able to diffuse for >48 hours between time of perfusion and brain fixation.

Fig S5. Additional examples of localization of PSEM and MiniRuby to CA1 infusion site in Gad2Cre behavior cohort. (**A**) Additional confocal images taken at 20x (image on left) and 5X (images on right) magnification of coronal sections derived from Gad2-cre mice used for behavioral testing that had been injected in LEC with an AAV^{Cre} expressing PSAM-2A-GFP. The mice received an infusion of PSEM and miniRuby solution and were killed approximately 10 min after the end of the 5-min infusion period. Images show miniRuby (magenta in image on left, red in images on right) and DAPI (blue). (**B**) Zoomed in image of left image of A, showing miniRuby (magenta) overlap of GFP (green) expressing fibers in SLM/SR border of CA1.

Fig S6. Hippocampal-specific targeting of LEC LRIPs. (**A**) 20x magnification confocal image of coronal section derived from a Gad2Cre mouse injected in LEC with AAV^{Cre} expressing EGFP. Image shows expression of GFP was largely restricted to hippocampus, with few fibers in overlying neocortex. GFP in green and DAPI in blue. (**B**) Zoomed in image of area of interest indicated in (A) (white rectangle), showing LRIPs expressing GFP (green) in SLM/SR border of CA1 and DAPI (blue). Note: Because the LRIPs are localized to hippocampus in this brain area, our local PSEM infusion, whose extent is indicated by the mRuby fluorescence in figs. S4 and S5, will selectively target LRIPs within hippocampus.

Fig. S7. No change in anxiety or locomotor behavior in the open-field test upon LEC LRIP silencing with PSEM/PSAM. (**A**) Number of rearing events (±SEM) of mice in an open field 5 min after infusion with PSEM (0.5 μl of 15 μM solution). The mice expressed either GFP or PSAM in LEC. (**B** to **D**) Total path length (B), portion of path length restricted to perimeter (C), and portion of path length restricted to the center (D) of open field. There was no significant difference between the control group, expressing GFP in the LRIPs, and the LRIP-silenced group, expressing PSAM ($P = 0.3426$, Distance covered; $P = 0.3557$, Rearing events). PSEM was applied to the CA1 region of both groups using a cannula. (**E** and **F**) Bar plots of time spent with object A and B by mice in the control and PSEM groups in Trial 1 (E) and Trial 2 (F). In trial 1, mice were exposed to object A (green circle) and object B (magenta triangle) for 10 min. Following a 3-min intertrial interval, mice were again exposed to the same pair of objects for trial 2. The mice were then tested for object recognition memory after a 10-min interval by replacing either object A or object B with object C (orange hexagon), the novel object. Mice in which LEC LRIPs were silenced with PSEM infusion spent more time with the objects in trial 2 compared with the control group (Object A, Control, 25.30 ± 4.92 s; +PSEM, 87.7 ± 27.96 s, $P < 0.05$, *t* test; Object B, Control, 23.49 ± 5.17 s; +PSEM, 53.84 ± 19.08 s; $P < 0.05$, *t* test).

Fig. S8. GCaMP6f Ca^{2+} signals in LEC LRIPs in SLM region of CA1 in response to sensory input and behavior. (**A**) 10X tile scan of a whole brain section, and (**B**) 20X zoomed image of site of injection of AAV^{Cre} expressing GCaMP6f in LEC of left hemisphere from a GAD2-Cre mouse. $GCaMP6f^{+}$ cell bodies in green; DAPI channel in blue). (**C**) 20X image of hippocampus from left hemisphere (ipsilateral to LEC injection site) showing $tdTomato^{+}$ GABAergic interneuron soma and $GCaMP6f^{+}$ LRIP axons from LEC traversing SLM of CA1. (**D**) Histogram bar plots of the number of responsive boutons (*y* axis) as a function of the number of stimulus modalities (*x* axis) to which a given bouton responds, either with a single sensory stimulus (above) or two stimuli presented simultaneously (below). The experimental data is plotted in black while the distribution expected if the stimuli and bouton responses were independent is in gray. For single stimulus presentations, very few boutons respond to more than one type of stimulus, following the predictions for independent responses (P = 0.01659). In contrast, paired stimuli evoke Ca^{2+} responses in a greater than expected number of boutons ($P < 0.03$), perhaps the influence of a single overlapping stimulus in paired modalities (e.g. bouton responding to airpuff alone would likely respond to all three pairings with air, A+T; A+L, A+W). (**E**) Average Ca^{2+} responses (± SEM) elicited by behavioral activity of licking and running. Spontaneous responses (black) include all running or licking bouts observed in the absence of a closely-timed external stimulus (airpuff, water, tone, or light). Evoked responses (red) occurred synchronously with a particular stimulus. The rise time and peak of the $\Delta F/F$ Ca^{2+} signal is tightly time-locked to the stimulus presentation in the evoked lick and run PSTHs. (**F** to **H**) Time-averaged images of $tdTom^{+}$ IN soma and dendrites and $GCaMP^{+}$ LRIP axons and their terminals in CA1, depicting the ROIs for LRIP boutons (cyan) and an associated axon (yellow). Images (F) and schematic drawing (G) showing that LRIP boutons along a single axon may target different cellular compartments of CA1 INs, such as soma versus dendrite, as well as different cells. Images (H) and schematic drawing (**I**) showing LRIP boutons from more than one axon may target the same

CA1 IN. (G) Histogram frequency plot of $\Delta F/F$ peak Ca^{2+} responses (x axis) for LRIP boutons targeting $tdTom^{+}$ CA1 IN dendrites (magenta, mean $\Delta F/F$ = 0.086 ± 0.004, n = 278) or soma (green, $\Delta F/F$ = 0.03 ± 0.002, n = 91; significant response difference in dendrite- versus soma-targeting boutons, $P < 0.0001$) **I.** Relative frequency distribution of bouton-bouton Ca^{2+} response correlation coefficients for all identifiable bouton pairs originating from the same axon segment (solid blue, r = 0.488 ± 0.017, n = 808) versus boutons from different axons (cross-hatched red, r = 0.115 ± 0.009, n = 3992; $P < 0.0001$, Mann-Whitney U test). Response similarity was determined by calculating the z-scored response magnitude for each stimulus for each bouton and then comparing the responses of pairs of boutons by calculating the correlation between their responses across all stimuli.

Fig. S9. Cholecystokinin-expressing (CCK) dendrite targeting interneurons are a major target of EC LRIPs in CA1. (**A**) 20X confocal tile scan image of a transverse hippocampal section depicting ChR2-$EYFP^{+}$ LRIP inputs from MEC and LEC (green) and anti-mouse CCK ab immunostaining (magenta). A Gad2-Cre mouse was injected with AAV^{Cre} in MEC and LEC to express ChR2 in all EC Cre^{+} GABAergic neurons. Hippocampal slices from these mice were first used for slice electrophysiology to map GABAergic connectivity between EC and CA1, followed by resectioning and immunostaining post-fixation. Mouse anti-CCK labeled IN soma in the SR/SLM border showing close proximity to LRIP axons are indicated with white arrowheads. (**B**) Inset shows a 60X zoomed in image of LRIP axon terminals (white) impinging on a CCK immunopositive cell body (magenta) located in SLM of CA1. (**C**) Neuronal tracing-based reconstruction of a putative CCK IN (magenta) that receives direct GABAergic and glutamatergic inputs from EC and glutamatergic inputs via SC. The CCK IN axon targets the dendrites of a dually-recorded CA1 PN (cyan). Both cells were intracellularly filled with biocytin during the recordings. The ChR2-$EYFP^{+}$ LRIP axons traced using fluorescence guidance are shown in green. Laser light was used to photostimulate these axons and evoke an IPSC in the filled IN. This particular

interneuron not only innervates the apical dendrite of the CA1 PN in SR and SLM but also sends axonal projections to DG, similar to a dendrite-targeting class of CCK INs identified *in vivo* in a previous study (*47*). (**D** and **E**) Representative neuronal reconstructions of CA1 INs that receive LEC LRIPs, as determined by the presence of IPSCs recorded in the IN soma in response to photostimulation of ChR2-EYFP^{+} LRIP axons. The morphology of both INs is prototypical of SC-associated CCK INs targeting CA1 PN dendrites (*29*, *47*, *61–66*).

Fig. S10. CA1 PN dendritic depolarization and Ca^{2+} signaling with EC and SC stimulation. (**A**) Representative gray scale epifluorescence image of a CA1 PN filled with Alexa Fluor 594 through an intracellular patch pipette during whole-cell recording from the proximal apical dendrite (250 µm from the soma). Dendritic recordings for Fig. 6 F-H were performed at comparable locations. (**B**) Whole-cell voltage recordings from the proximal dendrite of a CA1 PN of PSPs elicited by electrical stimulation of EC and SC inputs with inhibition intact (blue) or blocked with SR, CGP (red). (**C**) Floating bar (Mean ± SEM) and scatter plot (individual cells) of PSP amplitude in proximal dendrites of CA1 PNs with EC and SC stimulation before and after application of GABAR blockers. With inhibition intact the average EC depolarizing PSP is 1.02 ± 0.24 mV, which increased to 4.43 ± 0.11 mV with GABARs blocked ($P < 0.001$, two-tailed paired *t* test, $n = 6$). For SC input stimulation, average PSP amplitude was 4.75 ± 0.56 mV with inhibition intact and 8.87 ± 1.03 mV with inhibition blocked ($P = 0.0011$, two-tailed paired *t* test, $n = 6$). (**D**) Upper inset shows an example image of an Alexa-filled CA1 PN dendrite in stratum radiatum, showing the path for line scanning (red) of fluorescence signal in four dendritic spines (numbered 1-4). Ca^{2+} transient from one spine (green) measured from Fluo5F fluorescence change (dF/F) in response to a single EC-SC paired stimulation at a 20-ms interval (EC before SC). Lower panel shows green (Fluo-5F) and red (Alexa fluor 594) channel overlay line scans in 4 spines in response to the paired stimulation. (**E**) Mean ratiometric Ca^{2+} responses (ΔG/R, ± SEM) recorded from proximal dendritic

spines of CA1 PN upon stimulation of SC input alone (blue diagonal hatched**,** ΔG/R = 1.02 ± 0.25, *n* = 5), single paired stimulation of EC-SC inputs at a 20-ms interval (black; ΔG/R = 2.15 ± 0.34, *n* = 5) versus 10 ms (gray; ΔG/R 1.29 ± 0.11, *n* = 5) pairing intervals. The Ca2+ signal evoked by EC-SC pairing with a 20-ms interval is significantly larger than that evoked by SC stimulation alone (*P* < 0.001, *t* test) or pairing at a 10-ms interval (*P* < 0.0001, *t* test). (**F**) Two-photon 2-D scan image (left) of a CA1 PN intracellularly filled with Alexa Fluor 594 (red) and Fluo-5F (green) showing the Ca^{2+} signal (merged in yellow) in response to a train of -20 ms paired EC-SC stimuli delivered at 1 Hz. (**G**) Mean ratiometric Ca^{2+} responses (ΔG/R, ± SEM) recorded from proximal dendritic spines (solid blue, ΔG/R = 4.7 ± 0.35, *n* = 15), dendritic shaft (cross hatched magenta, ΔG/R = 2.63 ± 0.32, *n* = 5) and soma (diagonal hatched green, Δ G/R = 1.44 ± 0.43, *n* = 5) of CA1 PNs immediately after a 90 s period of 1 Hz EC-SC stimulation at a –20-ms pairing interval. The color-coded scan locations are indicated in (F).

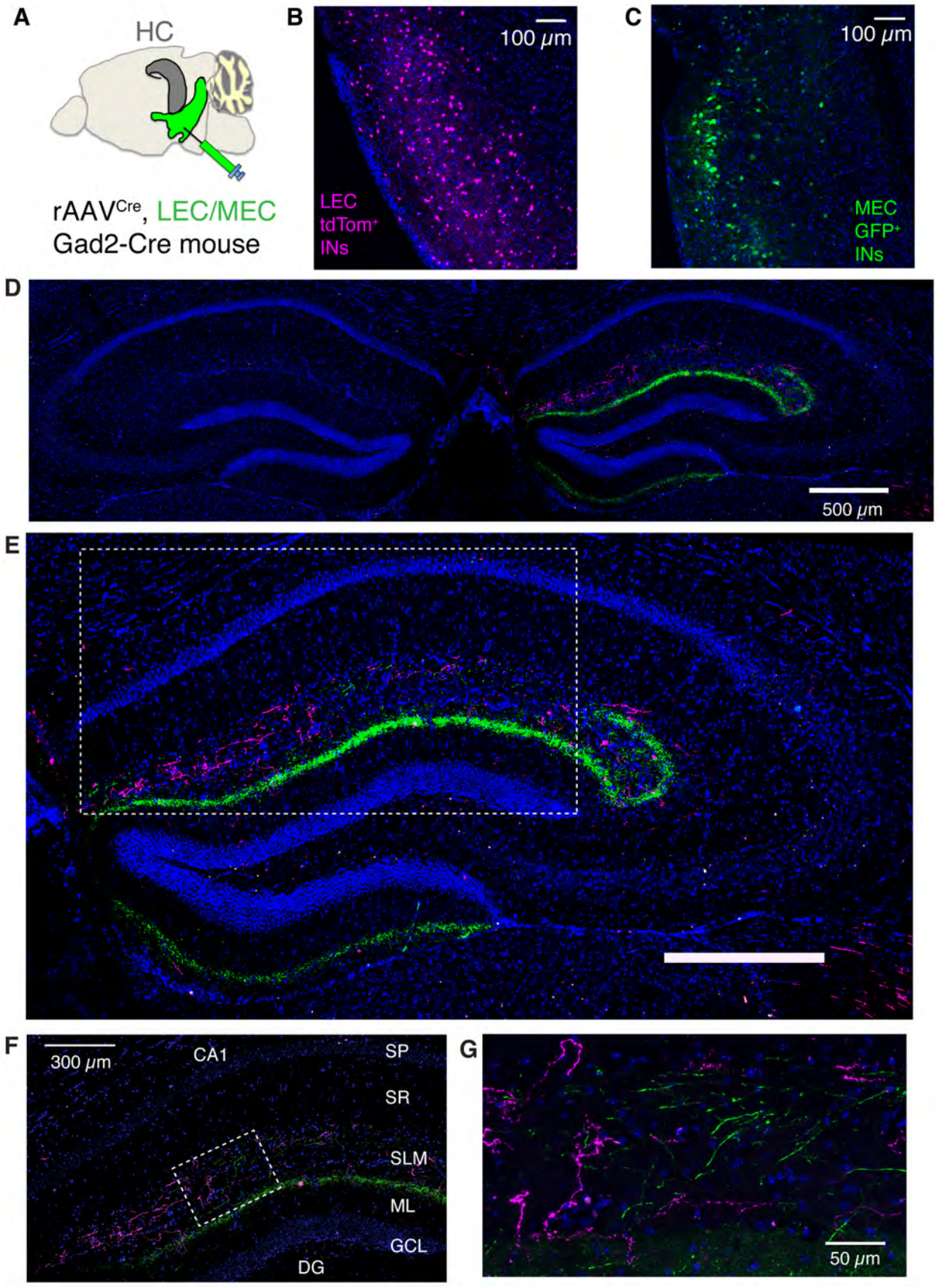
A
HC
rAAVCre, LEC/MEC
Gad2-Cre mouse
B
100 μm
LEC
tdTom+
INs
C
100 μm
MEC
GFP+
INs
D
500 μm
E
F
300 μm
CA1
SP
SR
SLM
ML
GCL
DG
G
50 μm

Fig. S1

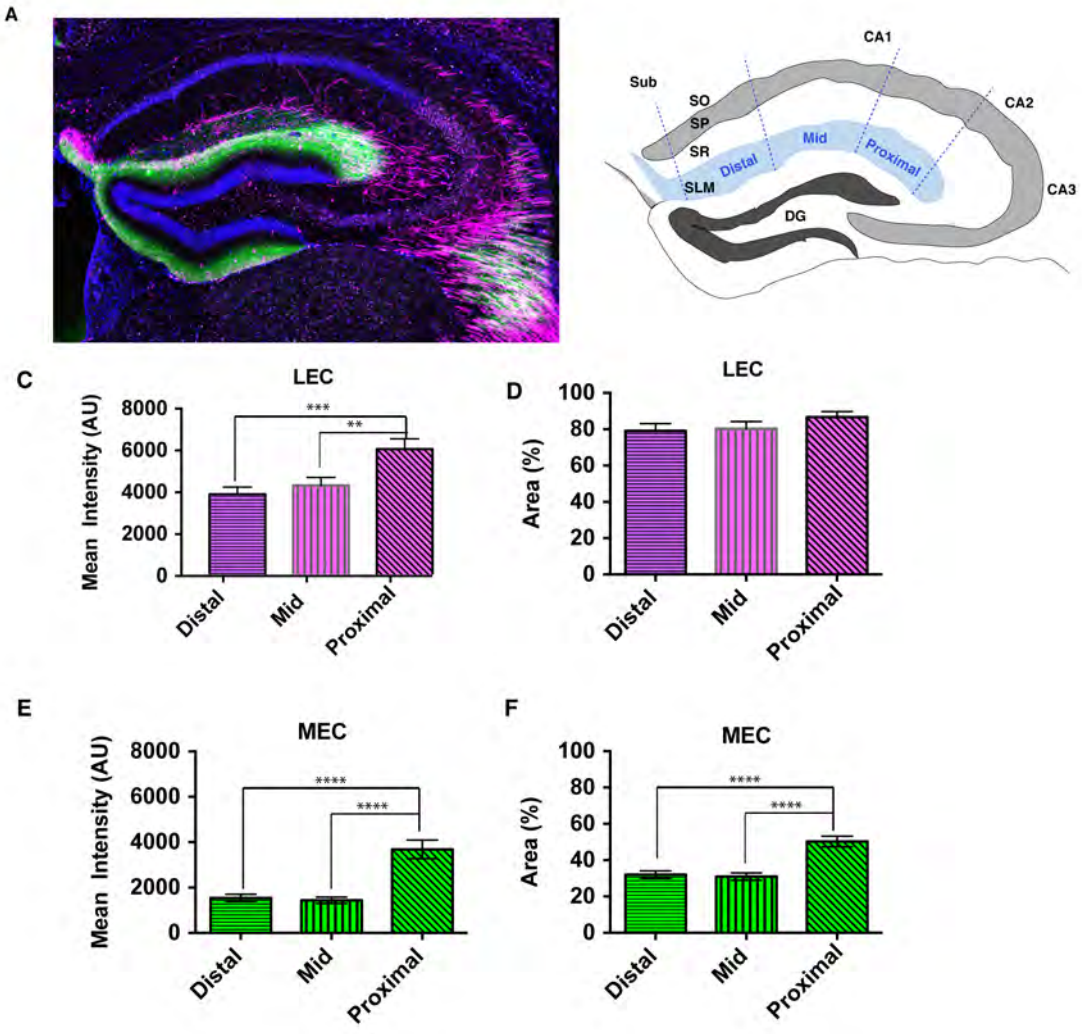
A
CA1
Sub
SO
SP
SR
SLM
Distal
Mid
Proximal
CA2
CA3
DG
C
LEC
Mean Intensity (AU)
8000
6000
4000
2000
0
***
**
Distal
Mid
Proximal
D
LEC
Area (%)
100
80
60
40
20
0
Distal
Mid
Proximal
E
MEC
Mean Intensity (AU)
8000
6000
4000
2000
0
****
****
Distal
Mid
Proximal
F
MEC
Area (%)
100
80
60
40
20
0
****
****
Distal
Mid
Proximal

Fig. S2

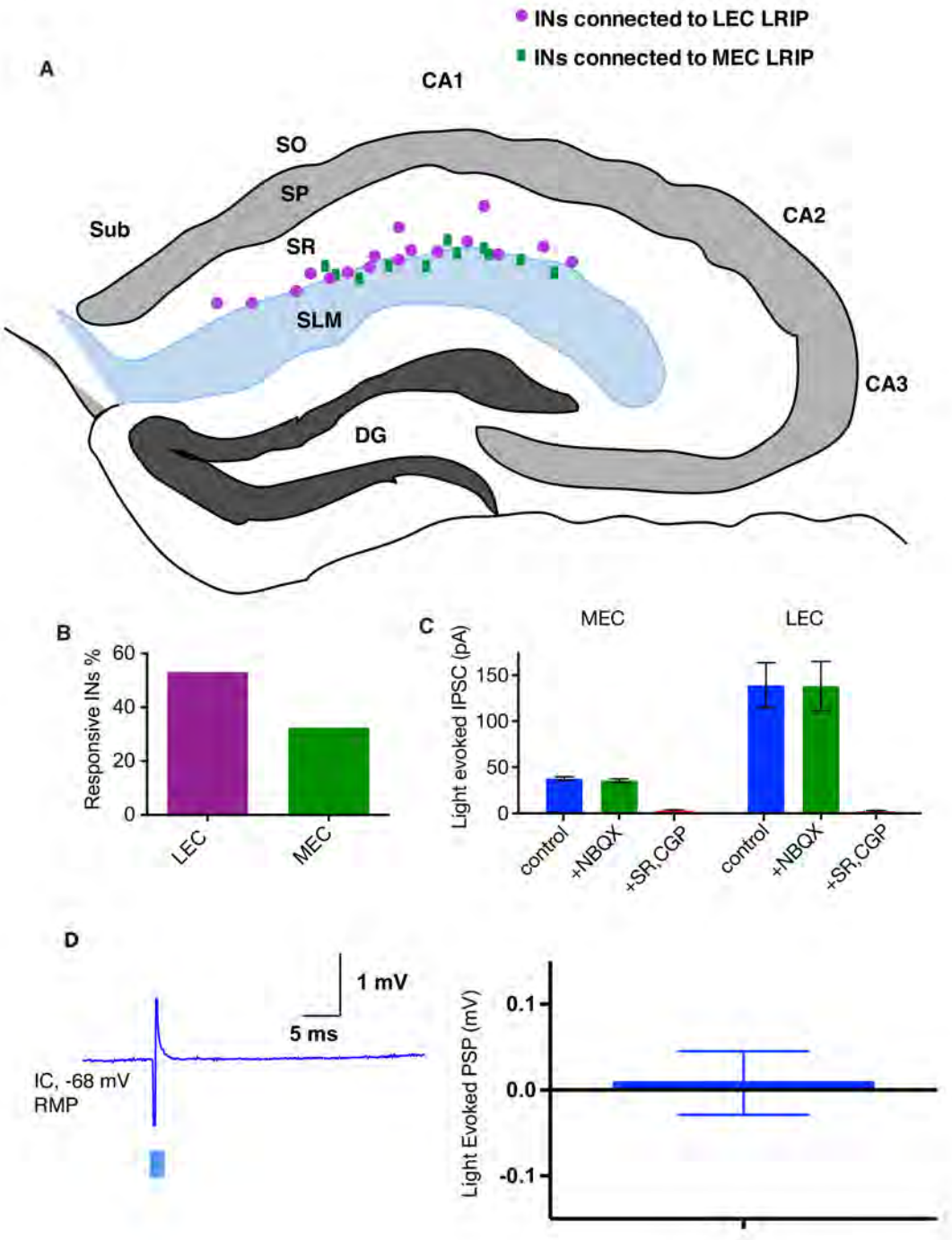
INs connected to LEC LRIP
INs connected to MEC LRIP
A
CA1
SO
SP
SR
SLM
Sub
CA2
CA3
DG
B
Responsive INs %
60
40
20
0
LEC
MEC
C
MEC
LEC
Light evoked IPSC (pA)
150
100
50
0
control
+NBQX
+SR,CGP
control
+NBQX
+SR,CGP
D
1 mV
5 ms
IC, -68 mV
RMP
Light Evoked PSP (mV)
0.1
0.0
-0.1

Fig. S3

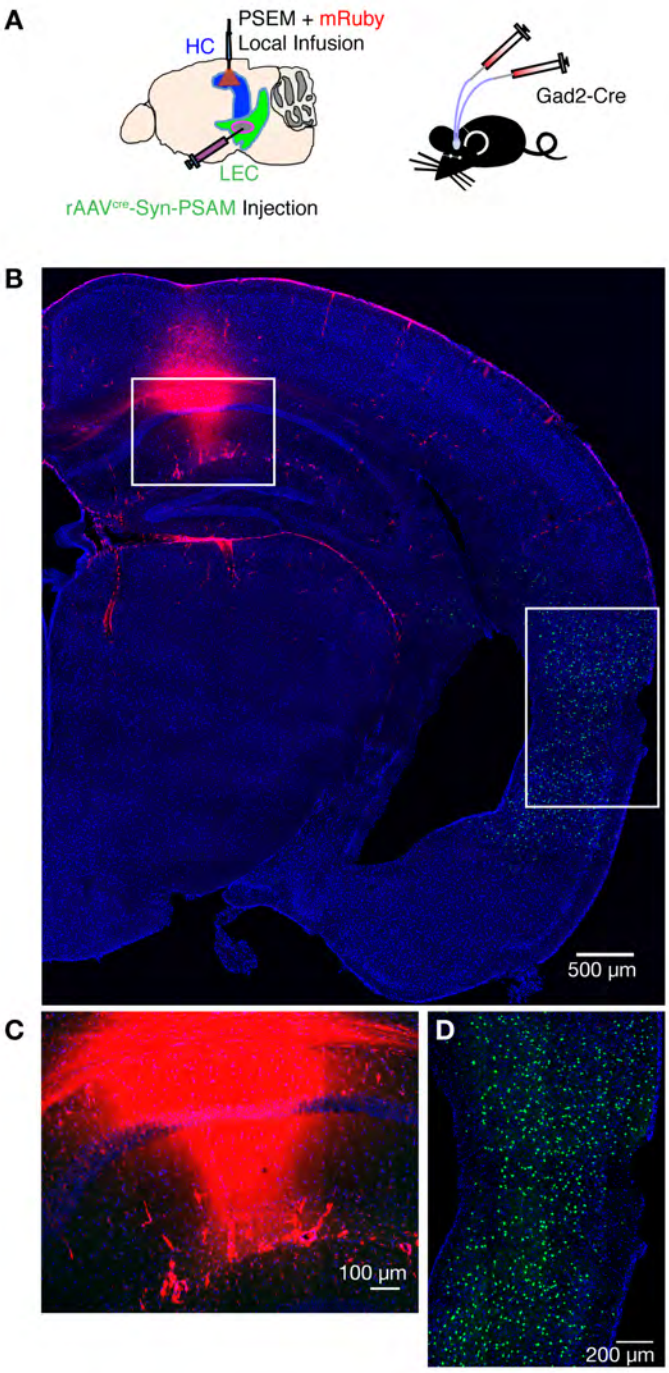
A
PSEM + mRuby
Local Infusion
HC
LEC
rAAV^cre-Syn-PSAM Injection
Gad2-Cre
B
500 µm
C
100 µm
D
200 µm

Fig. S4

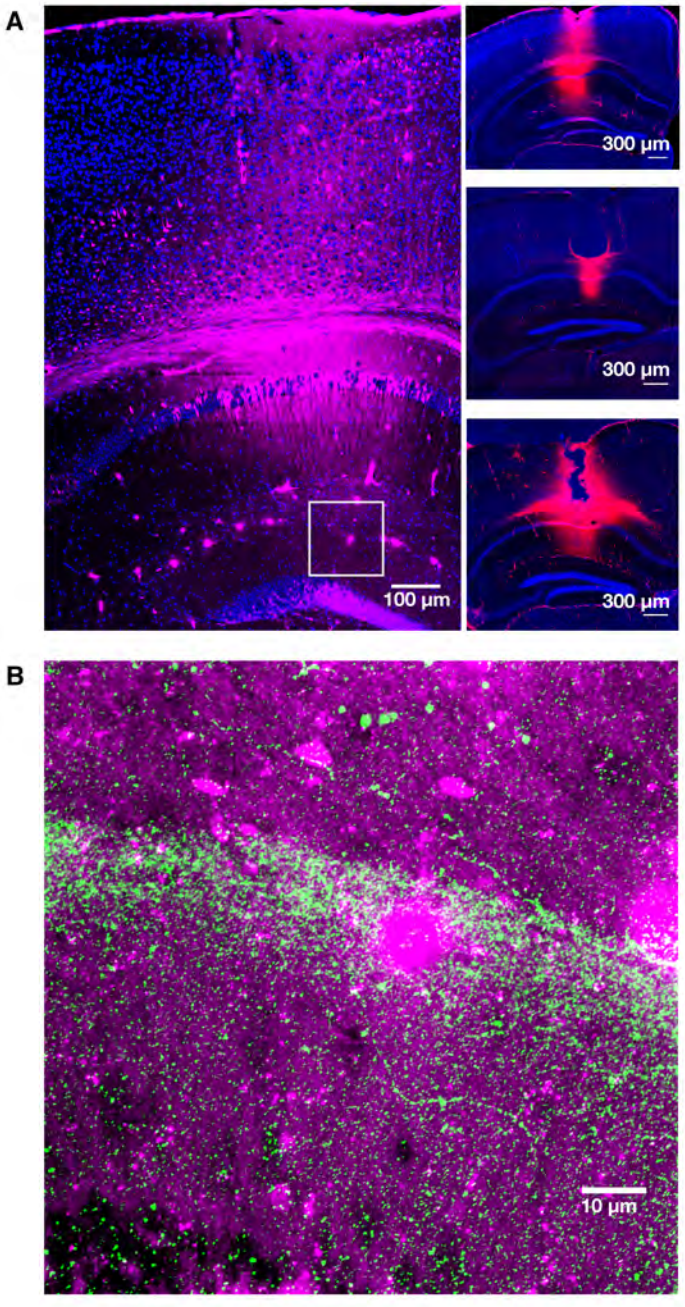

Fig. S5

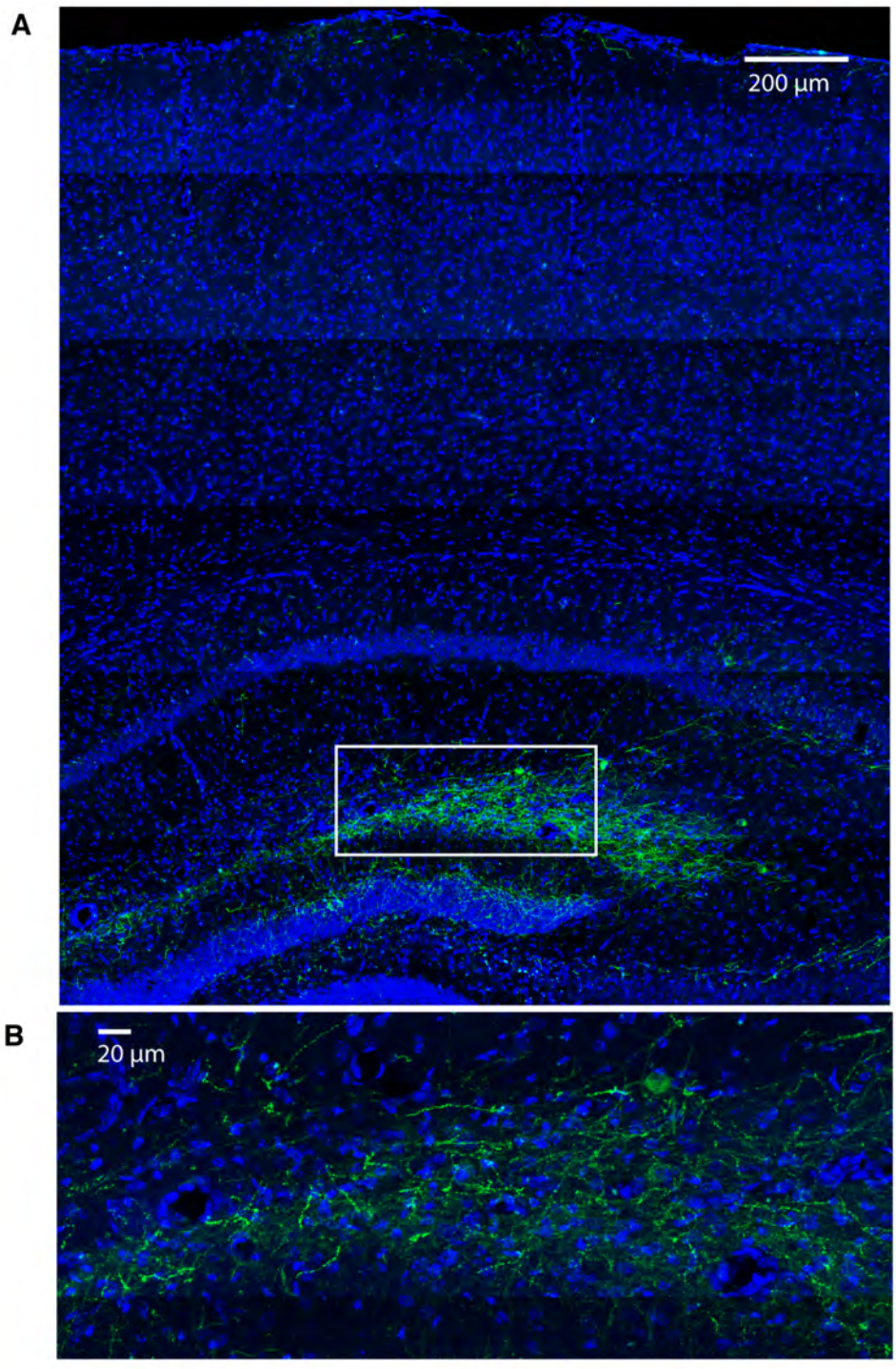

Fig. S6

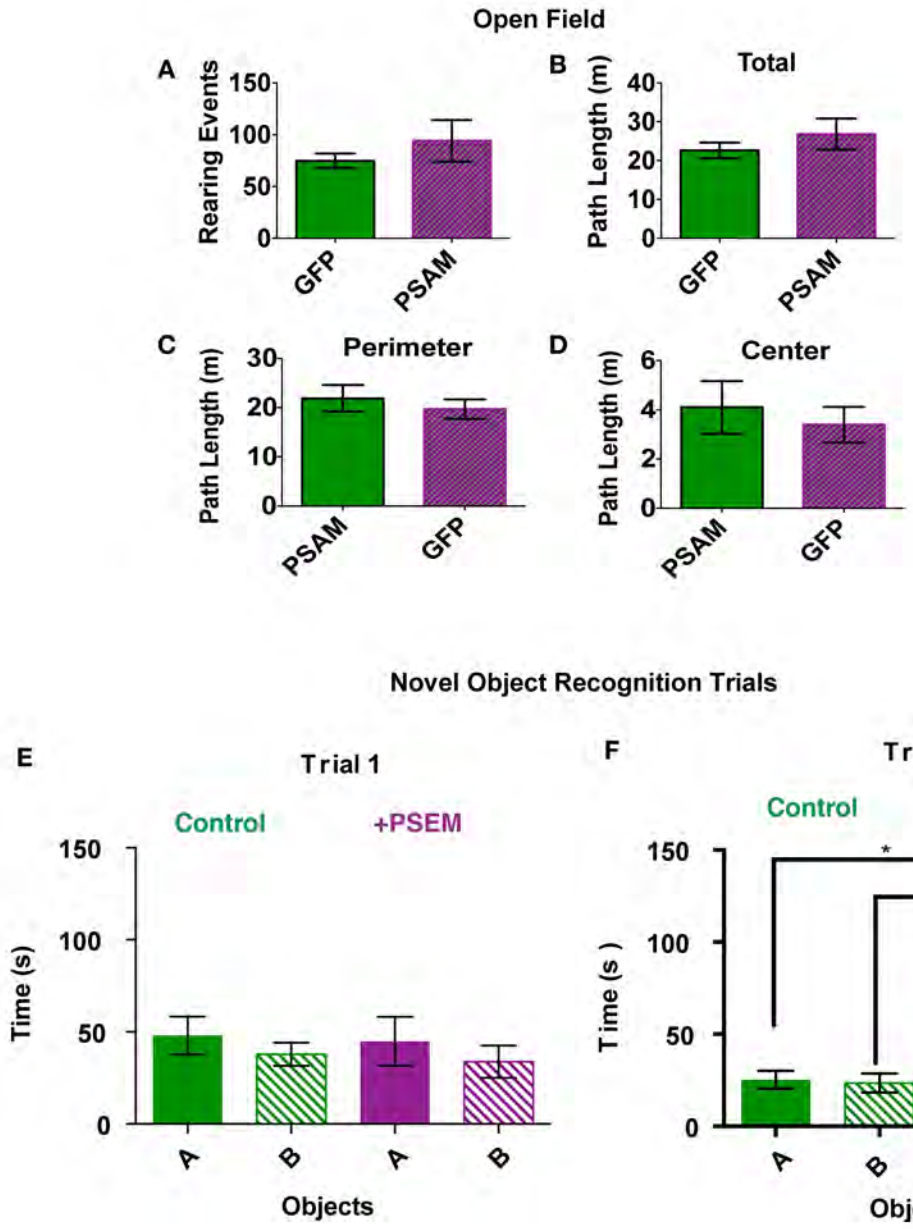
Open Field
A
Rearing Events
150
100
50
0
GFP
PSAM
B
Total
Path Length (m)
40
30
20
10
0
GFP
PSAM
C
Perimeter
Path Length (m)
30
20
10
0
PSAM
GFP
D
Center
Path Length (m)
6
4
2
0
PSAM
GFP
Novel Object Recognition Trials
E
Trial 1
Control
+PSEM
Time (s)
150
100
50
0
A
B
A
B
Objects
F
Trial 2
Control
+PSEM
*
*
Time (s)
150
100
50
0
A
B
A
B
Objects

Fig. S7

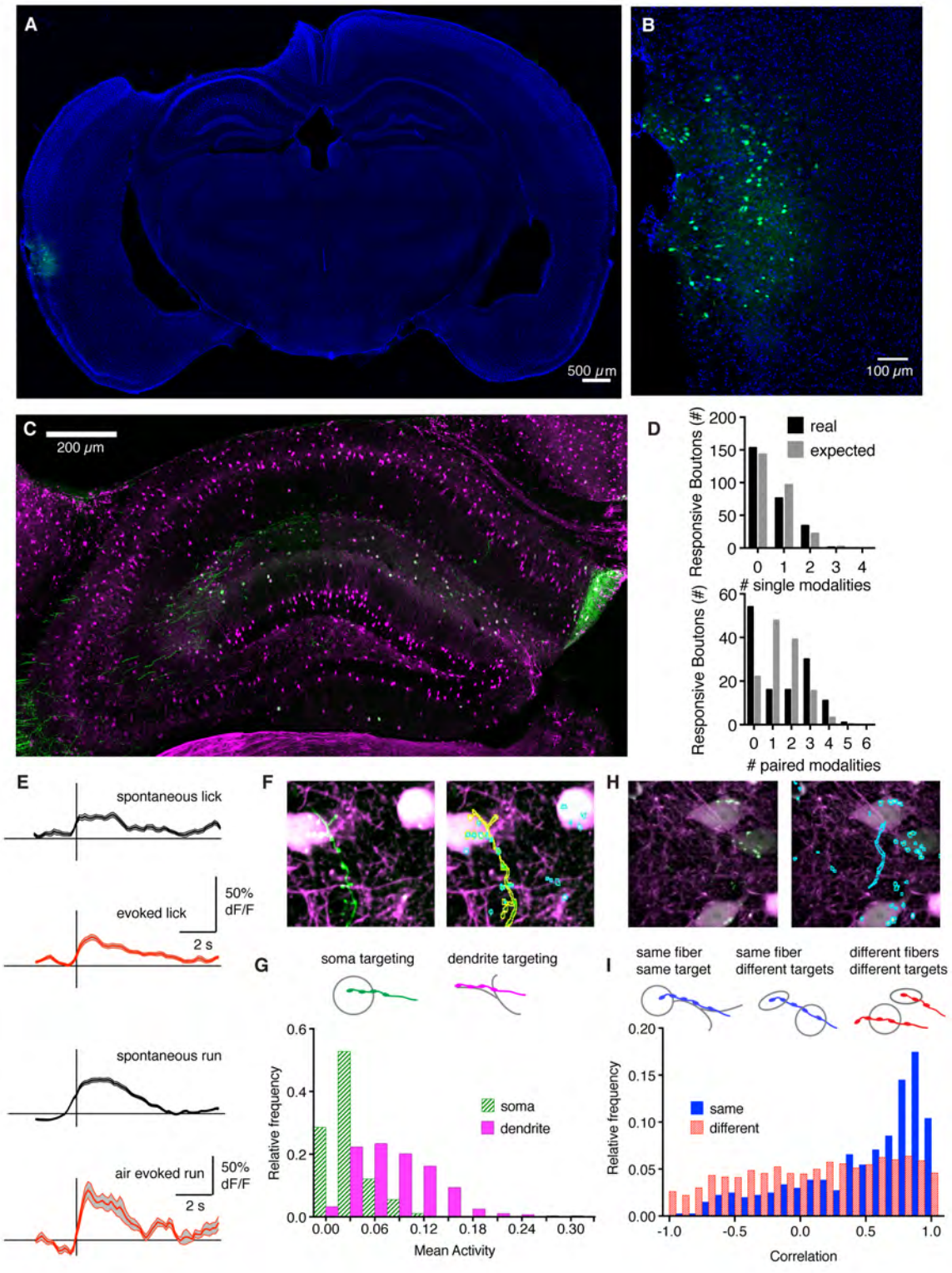
A
500 μm
B
100 μm
C
200 μm
D
real
expected
Responsive Boutons (#)
single modalities
paired modalities
E
spontaneous lick
evoked lick
50% dF/F
2 s
spontaneous run
air evoked run
F
G
soma targeting
dendrite targeting
soma
dendrite
Relative frequency
Mean Activity
H
I
same fiber same target
same fiber different targets
different fibers different targets
same
different
Correlation

Fig. S8

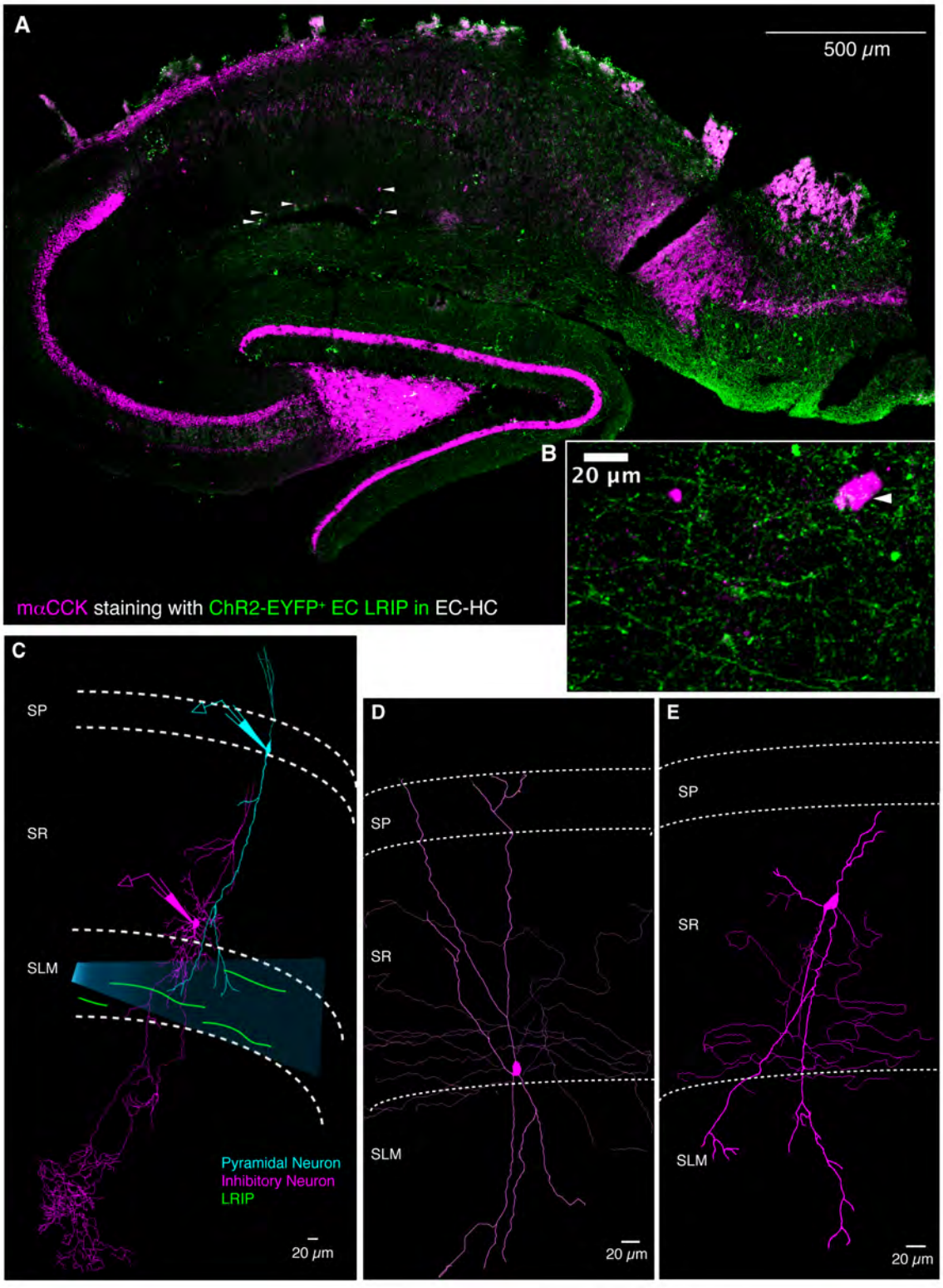
A
500 μm
mαCCK staining with ChR2-EYFP+ EC LRIP in EC-HC
B
20 μm
C
SP
SR
SLM
Pyramidal Neuron
Inhibitory Neuron
LRIP
20 μm
D
SP
SR
SLM
20 μm
E
SP
SR
SLM
20 μm

Fig. S9

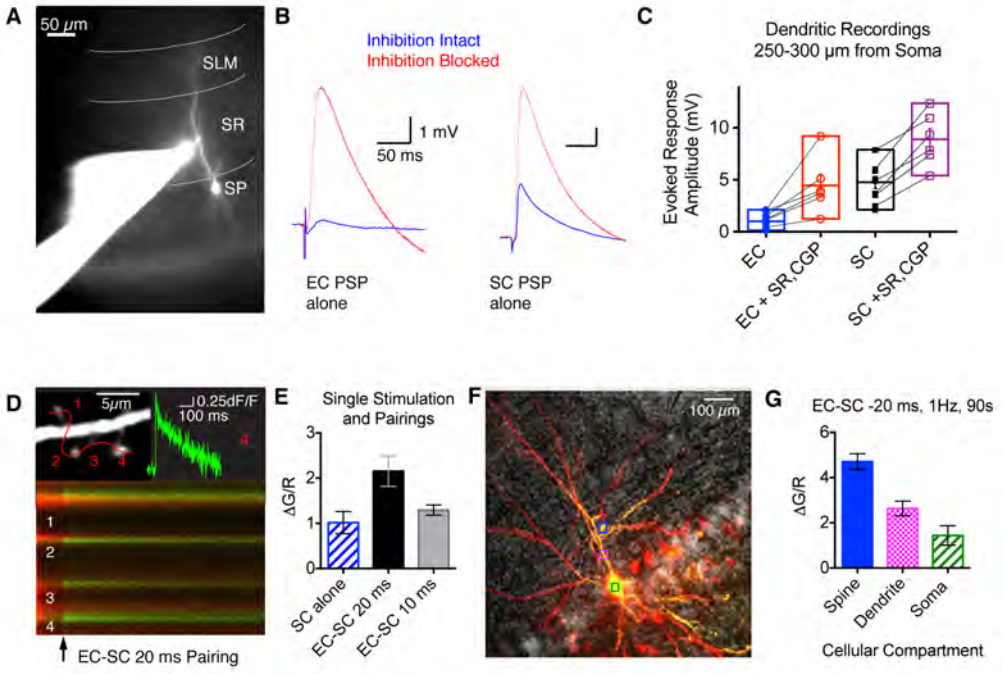
A
50 μm
SLM
SR
SP
B
Inhibition Intact
Inhibition Blocked
1 mV
50 ms
EC PSP
alone
SC PSP
alone
C
Dendritic Recordings
250-300 μm from Soma
Evoked Response
Amplitude (mV)
10
5
0
EC
EC + SR,CGP
SC
SC +SR,CGP
D
5μm
0.25dF/F
100 ms
1
2
3
4
EC-SC 20 ms Pairing
E
Single Stimulation
and Pairings
ΔG/R
3
2
1
0
SC alone
EC-SC 20 ms
EC-SC 10 ms
F
100 μm
G
EC-SC -20 ms, 1Hz, 90s
ΔG/R
6
4
2
0
Spine
Dendrite
Soma
Cellular Compartment

Fig. S10

Movie S1. In vivo imaging showing activation of LRIP boutons in SLM on presentation of water rewards. Time averaged image showing GCaMP labeled LEC LRIP boutons (green) terminating on $tdTom^+$ GABAergic interneuron cell bodies and dendrites (magenta) in SLM of CA1 (upper left). Video showing Ca^{2+} signals (principal component analysis, color calibrated white/red - high; blue low $\Delta F/F$) in the LRIP terminals of 5 trials as they get activated when the mouse receives a water reward. The presentation of the water reward is indicated (red) apposed with time synched video plots of the behavioral responses of the mouse namely, the run signal (blue) and the lick response (green) as a function of time (s) for each trial.

REFERENCES AND NOTES

1. V. H. Brun, S. Leutgeb, H. Q. Wu, R. Schwarcz, M. P. Witter, E. I. Moser, M. B. Moser, Impaired spatial representation in CA1 after lesion of direct input from entorhinal cortex. *Neuron* **57**, 290–302 (2008). Medline doi:10.1016/j.neuron.2007.11.034

2. J. Suh, A. J. Rivest, T. Nakashiba, T. Tominaga, S. Tonegawa, Entorhinal cortex layer III input to the hippocampus is crucial for temporal association memory. *Science* **334**, 1415–1420 (2011). Medline doi:10.1126/science.1210125

3. T. Kitamura, M. Pignatelli, J. Suh, K. Kohara, A. Yoshiki, K. Abe, S. Tonegawa, Island cells control temporal association memory. *Science* **343**, 896–901 (2014). Medline doi:10.1126/science.1244634

4. S. Melzer, M. Michael, A. Caputi, M. Eliava, E. C. Fuchs, M. A. Whittington, H. Monyer, Long-range-projecting GABAergic neurons modulate inhibition in hippocampus and entorhinal cortex. *Science* **335**, 1506–1510 (2012). Medline doi:10.1126/science.1217139

5. D. G. Amaral, M. P. Witter, The three-dimensional organization of the hippocampal formation: A review of anatomical data. *Neuroscience* **31**, 571–591 (1989). Medline doi:10.1016/0306-4522(89)90424-7

6. M. P. Witter, D. G. Amaral, Entorhinal cortex of the monkey: V. Projections to the dentate gyrus, hippocampus, and subicular complex. *J. Comp. Neurol.* **307**, 437–459 (1991). Medline doi:10.1002/cne.903070308

7. G. Buzsáki, Feed-forward inhibition in the hippocampal formation. *Prog. Neurobiol.* **22**, 131–153 (1984). Medline doi:10.1016/0301-0082(84)90023-6

8. T. Jarsky, A. Roxin, W. L. Kath, N. Spruston, Conditional dendritic spike propagation following distal synaptic activation of hippocampal CA1 pyramidal neurons. *Nat. Neurosci.* **8**, 1667–1676 (2005). Medline doi:10.1038/nn1599

9. H. Takahashi, J. C. Magee, Pathway interactions and synaptic plasticity in the dendritic tuft regions of CA1 pyramidal neurons. *Neuron* **62**, 102–111 (2009). Medline doi:10.1016/j.neuron.2009.03.007

10. J. T. Dudman, D. Tsay, S. A. Siegelbaum, A role for synaptic inputs at distal dendrites: Instructive signals for hippocampal long-term plasticity. *Neuron* **56**, 866–879 (2007). Medline doi:10.1016/j.neuron.2007.10.020

11. J. Basu, K. V. Srinivas, S. K. Cheung, H. Taniguchi, Z. J. Huang, S. A. Siegelbaum, A cortico-hippocampal learning rule shapes inhibitory microcircuit activity to enhance hippocampal information flow. *Neuron* **79**, 1208–1221 (2013). Medline doi:10.1016/j.neuron.2013.07.001

12. K. C. Bittner, C. Grienberger, S. P. Vaidya, A. D. Milstein, J. J. Macklin, J. Suh, S. Tonegawa, J. C. Magee, Conjunctive input processing drives feature selectivity in hippocampal CA1 neurons. *Nat. Neurosci.* **18**, 1133–1142 (2015). Medline doi:10.1038/nn.4062

13. V. H. Brun, M. K. Otnass, S. Molden, H. A. Steffenach, M. P. Witter, M. B. Moser, E. I. Moser, Place cells and place recognition maintained by direct entorhinal-hippocampal circuitry. *Science* **296**, 2243–2246 (2002). Medline doi:10.1126/science.1071089

14. M. Fyhn, S. Molden, M. P. Witter, E. I. Moser, M. B. Moser, Spatial representation in the entorhinal cortex. *Science* **305**, 1258–1264 (2004). Medline doi:10.1126/science.1099901

15. E. L. Hargreaves, G. Rao, I. Lee, J. J. Knierim, Major dissociation between medial and lateral entorhinal input to dorsal hippocampus. *Science* **308**, 1792–1794 (2005). Medline doi:10.1126/science.1110449

16. H. Taniguchi, M. He, P. Wu, S. Kim, R. Paik, K. Sugino, D. Kvitsiani, Y. Fu, J. Lu, Y. Lin, G. Miyoshi, Y. Shima, G. Fishell, S. B. Nelson, Z. J. Huang, A resource of Cre driver lines for genetic targeting of GABAergic neurons in cerebral cortex. *Neuron* **71**, 995–1013 (2011). Medline doi:10.1016/j.neuron.2011.07.026

17. E. S. Boyden, F. Zhang, E. Bamberg, G. Nagel, K. Deisseroth, Millisecond-timescale, genetically targeted optical control of neural activity. *Nat. Neurosci.* **8**, 1263–1268 (2005). Medline doi:10.1038/nn1525

18. S. Maren, K. L. Phan, I. Liberzon, The contextual brain: Implications for fear conditioning, extinction and psychopathology. *Nat. Rev. Neurosci.* **14**, 417–428 (2013). Medline doi:10.1038/nrn3492

19. C. J. Magnus, P. H. Lee, D. Atasoy, H. H. Su, L. L. Looger, S. M. Sternson, Chemical and genetic engineering of selective ion channel-ligand interactions. *Science* **333**, 1292–1296 (2011). Medline doi:10.1126/science.1206606

20. F. L. Hitti, S. A. Siegelbaum, The hippocampal CA2 region is essential for social memory. *Nature* **508**, 88–92 (2014). Medline doi:10.1038/nature13028

21. S. J. Cohen, R. W. Stackman Jr., Assessing rodent hippocampal involvement in the novel object recognition task. A review. *Behav. Brain Res.* **285**, 105–117 (2015). Medline doi:10.1016/j.bbr.2014.08.002

22. R. E. Clark, S. M. Zola, L. R. Squire, Impaired recognition memory in rats after damage to the hippocampus. *J. Neurosci.* **20**, 8853–8860 (2000). Medline

23. J. A. Ainge, C. Heron-Maxwell, P. Theofilas, P. Wright, L. de Hoz, E. R. Wood, The role of the hippocampus in object recognition in rats: Examination of the influence of task parameters and lesion size. *Behav. Brain Res.* **167**, 183–195 (2006). Medline doi:10.1016/j.bbr.2005.09.005

24. S. J. Cohen, A. H. Munchow, L. M. Rios, G. Zhang, H. N. Asgeirsdóttir, R. W. Stackman Jr., The rodent hippocampus is essential for nonspatial object memory. *Curr. Biol.* **23**, 1685–1690 (2013). Medline doi:10.1016/j.cub.2013.07.002

25. C. A. Denny, N. S. Burghardt, D. M. Schachter, R. Hen, M. R. Drew, 4- to 6-week-old adult-born hippocampal neurons influence novelty-evoked exploration and contextual fear conditioning. *Hippocampus* **22**, 1188–1201 (2012). Medline doi:10.1002/hipo.20964

26. T. W. Chen, T. J. Wardill, Y. Sun, S. R. Pulver, S. L. Renninger, A. Baohan, E. R. Schreiter, R. A. Kerr, M. B. Orger, V. Jayaraman, L. L. Looger, K. Svoboda, D. S. Kim,

Ultrasensitive fluorescent proteins for imaging neuronal activity. *Nature* **499**, 295–300 (2013). Medline doi:10.1038/nature12354

27. P. Kaifosh, M. Lovett-Barron, G. F. Turi, T. R. Reardon, A. Losonczy, Septo-hippocampal GABAergic signaling across multiple modalities in awake mice. *Nat. Neurosci.* **16**, 1182–1184 (2013). Medline doi:10.1038/nn.3482

28. M. Lovett-Barron, P. Kaifosh, M. A. Kheirbek, N. Danielson, J. D. Zaremba, T. R. Reardon, G. F. Turi, R. Hen, B. V. Zemelman, A. Losonczy, Dendritic inhibition in the hippocampus supports fear learning. *Science* **343**, 857–863 (2014). Medline doi:10.1126/science.1247485

29. D. W. Cope, G. Maccaferri, L. F. Márton, J. D. Roberts, P. M. Cobden, P. Somogyi, Cholecystokinin-immunopositive basket and Schaffer collateral-associated interneurones target different domains of pyramidal cells in the CA1 area of the rat hippocampus. *Neuroscience* **109**, 63–80 (2002). Medline doi:10.1016/S0306-4522(01)00440-7

30. T. Klausberger, P. Somogyi, Neuronal diversity and temporal dynamics: The unity of hippocampal circuit operations. *Science* **321**, 53–57 (2008). Medline doi:10.1126/science.1149381

31. H. Pawelzik, D. I. Hughes, A. M. Thomson, Physiological and morphological diversity of immunocytochemically defined parvalbumin- and cholecystokinin-positive interneurones in CA1 of the adult rat hippocampus. *J. Comp. Neurol.* **443**, 346–367 (2002). Medline doi:10.1002/cne.10118

32. S. H. Lee, I. Soltesz, Requirement for CB1 but not GABAB receptors in the cholecystokinin mediated inhibition of GABA release from cholecystokinin expressing basket cells. *J. Physiol.* **589**, 891–902 (2011). Medline doi:10.1113/jphysiol.2010.198499

33. M. I. Daw, L. Tricoire, F. Erdelyi, G. Szabo, C. J. McBain, Asynchronous transmitter release from cholecystokinin-containing inhibitory interneurons is widespread and target-cell independent. *J. Neurosci.* **29**, 11112–11122 (2009). Medline doi:10.1523/JNEUROSCI.5760-08.2009

34. N. L. Golding, N. Spruston, Dendritic sodium spikes are variable triggers of axonal action potentials in hippocampal CA1 pyramidal neurons. *Neuron* **21**, 1189–1200 (1998). Medline doi:10.1016/S0896-6273(00)80635-2

35. F. Gambino, S. Pagès, V. Kehayas, D. Baptista, R. Tatti, A. Carleton, A. Holtmaat, Sensory-evoked LTP driven by dendritic plateau potentials in vivo. *Nature* **515**, 116–119 (2014). Medline doi:10.1038/nature13664

36. N. L. Golding, N. P. Staff, N. Spruston, Dendritic spikes as a mechanism for cooperative long-term potentiation. *Nature* **418**, 326–331 (2002). Medline doi:10.1038/nature00854

37. M. E. Larkum, J. J. Zhu, B. Sakmann, A new cellular mechanism for coupling inputs arriving at different cortical layers. *Nature* **398**, 338–341 (1999). Medline doi:10.1038/18686

38. G. Buzsáki, E. I. Moser, Memory, navigation and theta rhythm in the hippocampal-entorhinal system. *Nat. Neurosci.* **16**, 130–138 (2013). Medline doi:10.1038/nn.3304

39. A. Kamondi, L. Acsády, G. Buzsáki, Dendritic spikes are enhanced by cooperative network activity in the intact hippocampus. *J. Neurosci.* **18**, 3919–3928 (1998). Medline

40. A. Losonczy, J. K. Makara, J. C. Magee, Compartmentalized dendritic plasticity and input feature storage in neurons. *Nature* **452**, 436–441 (2008). Medline doi:10.1038/nature06725

41. M. E. Sheffield, D. A. Dombeck, Calcium transient prevalence across the dendritic arbour predicts place field properties. *Nature* **517**, 200–204 (2015). Medline doi:10.1038/nature13871

42. S. Royer, B. V. Zemelman, A. Losonczy, J. Kim, F. Chance, J. C. Magee, G. Buzsáki, Control of timing, rate and bursts of hippocampal place cells by dendritic and somatic inhibition. *Nat. Neurosci.* **15**, 769–775 (2012). Medline doi:10.1038/nn.3077

43. L. Roux, G. Buzsáki, Tasks for inhibitory interneurons in intact brain circuits. *Neuropharmacology* **88**, 10–23 (2015). Medline doi:10.1016/j.neuropharm.2014.09.011

44. A. J. Murray, J. F. Sauer, G. Riedel, C. McClure, L. Ansel, L. Cheyne, M. Bartos, W. Wisden, P. Wulff, Parvalbumin-positive CA1 interneurons are required for spatial working but not for reference memory. *Nat. Neurosci.* **14**, 297–299 (2011). Medline doi:10.1038/nn.2751

45. F. Donato, S. B. Rompani, P. Caroni, Parvalbumin-expressing basket-cell network plasticity induced by experience regulates adult learning. *Nature* **504**, 272–276 (2013). Medline doi:10.1038/nature12866

46. S. Hefft, P. Jonas, Asynchronous GABA release generates long-lasting inhibition at a hippocampal interneuron-principal neuron synapse. *Nat. Neurosci.* **8**, 1319–1328 (2005). Medline doi:10.1038/nn1542

47. T. Klausberger, L. F. Marton, J. O'Neill, J. H. Huck, Y. Dalezios, P. Fuentealba, W. Y. Suen, E. Papp, T. Kaneko, M. Watanabe, J. Csicsvari, P. Somogyi, Complementary roles of cholecystokinin- and parvalbumin-expressing GABAergic neurons in hippocampal network oscillations. *J. Neurosci.* **25**, 9782–9793 (2005). Medline doi:10.1523/JNEUROSCI.3269-05.2005

48. W. Jacob, R. Marsch, G. Marsicano, B. Lutz, C. T. Wotjak, Cannabinoid CB1 receptor deficiency increases contextual fear memory under highly aversive conditions and long-term potentiation in vivo. *Neurobiol. Learn. Mem.* **98**, 47–55 (2012). Medline doi:10.1016/j.nlm.2012.04.008

49. M. F. Yeckel, T. W. Berger, Feedforward excitation of the hippocampus by afferents from the entorhinal cortex: Redefinition of the role of the trisynaptic pathway. *Proc. Natl. Acad. Sci. U.S.A.* **87**, 5832–5836 (1990). Medline doi:10.1073/pnas.87.15.5832

50. E. W. Schomburg, A. Fernández-Ruiz, K. Mizuseki, A. Berényi, C. A. Anastassiou, C. Koch, G. Buzsáki, Theta phase segregation of input-specific gamma patterns in entorhinal-hippocampal networks. *Neuron* **84**, 470–485 (2014). Medline doi:10.1016/j.neuron.2014.08.051

51. J. J. Chrobak, A. Lörincz, G. Buzsáki, Physiological patterns in the hippocampo-entorhinal cortex system. *Hippocampus* **10**, 457–465 (2000). Medline doi:10.1002/1098-1063(2000)10:4<457::AID-HIPO12>3.0.CO;2-Z

52. K. M. Igarashi, L. Lu, L. L. Colgin, M. B. Moser, E. I. Moser, Coordination of entorhinal-hippocampal ensemble activity during associative learning. *Nature* **510**, 143–147 (2014). Medline doi:10.1038/nature13162

53. T. Nakashiba, J. Z. Young, T. J. McHugh, D. L. Buhl, S. Tonegawa, Transgenic inhibition of synaptic transmission reveals role of CA3 output in hippocampal learning. *Science* **319**, 1260–1264 (2008). Medline doi:10.1126/science.1151120

54. S. Hippenmeyer, E. Vrieseling, M. Sigrist, T. Portmann, C. Laengle, D. R. Ladle, S. Arber, A developmental switch in the response of DRG neurons to ETS transcription factor signaling. *PLOS Biol.* **3**, e159 (2005). Medline doi:10.1371/journal.pbio.0030159

55. L. Madisen, T. A. Zwingman, S. M. Sunkin, S. W. Oh, H. A. Zariwala, H. Gu, L. L. Ng, R. D. Palmiter, M. J. Hawrylycz, A. R. Jones, E. S. Lein, H. Zeng, A robust and high-throughput Cre reporting and characterization system for the whole mouse brain. *Nat. Neurosci.* **13**, 133–140 (2010). Medline doi:10.1038/nn.2467

56. G. Miyoshi, J. Hjerling-Leffler, T. Karayannis, V. H. Sousa, S. J. Butt, J. Battiste, J. E. Johnson, R. P. Machold, G. Fishell, Genetic fate mapping reveals that the caudal ganglionic eminence produces a large and diverse population of superficial cortical interneurons. *J. Neurosci.* **30**, 1582–1594 (2010). Medline doi:10.1523/JNEUROSCI.4515-09.2010

57. M. Yamamoto, N. A. Shook, O. Kanisicak, S. Yamamoto, M. N. Wosczyna, J. R. Camp, D. J. Goldhamer, A multifunctional reporter mouse line for Cre- and FLP-dependent lineage analysis. *Genesis* **47**, 107–114 (2009). Medline doi:10.1002/dvg.20474

58. F. Zhang, V. Gradinaru, A. R. Adamantidis, R. Durand, R. D. Airan, L. de Lecea, K. Deisseroth, Optogenetic interrogation of neural circuits: Technology for probing mammalian brain structures. *Nat. Protoc.* **5**, 439–456 (2010). Medline doi:10.1038/nprot.2009.226

59. J. V. Kupferman, J. Basu, M. J. Russo, J. Guevarra, S. K. Cheung, S. A. Siegelbaum, Reelin signaling specifies the molecular identity of the pyramidal neuron distal dendritic compartment. *Cell* **158**, 1335–1347 (2014). Medline doi:10.1016/j.cell.2014.07.035

60. A. Edelstein, N. Amodaj, K. Hoover, R. Vale, N. Stuurman, Computer control of microscopes using μManager. *Curr. Protoc. Mol. Biol.* Chap.: Unit 14.20 (2010). Medline

61. L. Tricoire, K. A. Pelkey, B. E. Erkkila, B. W. Jeffries, X. Yuan, C. J. McBain, A blueprint for the spatiotemporal origins of mouse hippocampal interneuron diversity. *J. Neurosci.* **31**, 10948–10970 (2011). Medline doi:10.1523/JNEUROSCI.0323-11.2011

62. P. Kaifosh, J. D. Zaremba, N. B. Danielson, A. Losonczy, SIMA: Python software for analysis of dynamic fluorescence imaging data. *Front. Neuroinform.* **8**, 80 (2014). Medline doi:10.3389/fninf.2014.00080

63. A. B. Ali, Presynaptic Inhibition of $GABA_A$ receptor-mediated unitary IPSPs by cannabinoid receptors at synapses between CCK-positive interneurons in rat hippocampus. *J. Neurophysiol.* **98**, 861–869 (2007). Medline doi:10.1152/jn.00156.2007

64. C. A. Cea-del Rio, J. J. Lawrence, F. Erdelyi, G. Szabo, C. J. McBain, Cholinergic modulation amplifies the intrinsic oscillatory properties of CA1 hippocampal cholecystokinin-positive interneurons. *J. Physiol.* **589**, 609–627 (2011). Medline doi:10.1113/jphysiol.2010.199422

65. T. J. Younts, V. Chevaleyre, P. E. Castillo, CA1 pyramidal cell theta-burst firing triggers endocannabinoid-mediated long-term depression at both somatic and dendritic inhibitory synapses. *J. Neurosci.* **33**, 13743–13757 (2013). Medline doi:10.1523/JNEUROSCI.0817-13.2013

66. S. H. Lee, C. Földy, I. Soltesz, Distinct endocannabinoid control of GABA release at perisomatic and dendritic synapses in the hippocampus. *J. Neurosci.* **30**, 7993–8000 (2010). Medline doi:10.1523/JNEUROSCI.6238-09.2010

67. I. Vida, K. Halasy, C. Szinyei, P. Somogyi, E. H. Buhl, Unitary IPSPs evoked by interneurons at the stratum radiatum-stratum lacunosum-moleculare border in the CA1 area of the rat hippocampus in vitro. *J. Physiol.* **506**, 755–773 (1998). Medline doi:10.1111/j.1469-7793.1998.755bv.x